Genetics of white color and iridophoroma in "Lemon Frost" leopard geckos

Longhua Guo[1,*], Joshua Bloom[1], Steve Sykes[2], Elaine Huang[3], Zain Kashif[1], Elise Pham[1], Katarina Ho[1], Ana Alcaraz[4], Xinshu Grace Xiao[3], Sandra Duarte-Vogel[5], Leonid Kruglyak[1,*]

[1]Department of Human Genetics, Department of Biological Chemistry, Howard Hughes Medical Institute, University of California, Los Angeles, CA 90095, USA

[2]Geckos Etc. Herpetoculture, Rocklin, CA 95765, USA

[3]Department of Integrative Biology and Physiology, University of California, Los Angeles, CA 90095, USA

[4]College of Veterinary Medicine, Western University of Health Sciences, Pomona, CA 91711, USA

[5]Division of Laboratory Animal Medicine, David Geffen School of Medicine, University of California, Los Angeles, CA 90095, USA

(*) To whom correspondence should be addressed: longhuaguo@mednet.ucla.edu; lkruglyak@mednet.ucla.edu

Abstract

Coloration patterns promote survival and reproductive success in the animal kingdom. Despite their importance, wide gaps exist in our understanding of the genetic and evolutionary mechanisms that underpin them. The leopard gecko[1], *Eublepharis macularius*, is a popular companion animal, and displays a variety of coloration patterns. We investigated a spontaneous semi-dominant mutation, known as "Lemon Frost", that causes extensive white color in leopard

gecko skin. Although "Lemon Frost" individuals are aesthetically appealing, more than 80% of them develop tumors of white color (*i.e.*, iridophoroma) 0.5 to 5 years after birth. To identify the gene that regulates white color and is likely also responsible for the iridophoroma, we genotyped 220 animals, including 33 homozygous mutants, with short-read sequencing. We used synteny, linkage analysis and homozygosity mapping to localize the mutation to a strong candidate gene, SPINT1[2,3], a tumor suppressor previously implicated in human skin cutaneous melanoma (SKCM) as well as in over-proliferation of epithelial cells in mice and zebrafish[4-16]. Our work establishes the leopard gecko as a tractable genetic system and suggests that a tumor suppressor in melanocytes in humans can also suppress tumor development in iridophores in lizards.

Introduction

Color-producing cells[17-21] contribute to animal coloration and patterns. Some cells, such as melanocytes, produce pigments chemically. Others, such as iridophores, produce colors structurally by making crystal platelets[22-25]. Iridophores are not present in mammals, but are widespread in insects, fish, birds, amphibians and reptiles. Different types of iridophores can lead to different colors, including blue[26,27] and white[28]. There have been few molecular genetic analyses of the regulation of chromatophores in cells other than melanocytes. A recent study found that endothelin signaling regulates iridophore development and proliferation in zebrafish[29]. In mammals, this pathway is required for melanocyte development[30], suggesting that signaling pathways conserved in evolution can be adapted to regulate different types of chromatophores.

Many reptile species (*e.g.*, geckos, chameleons, snakes) are bred in captivity as companion animals, and breeders have established morphs with unique colors and patterns[18]. The inheritance of different color morphs is usually carefully documented by breeders. The common leopard gecko, *Eublepharis macularius*, is an especially attractive model to study the molecular

regulation of coloration because dozens of color and pattern morphs have been established over the past 30 years of selective breeding. These morphs either intensify a particular color (Supplementary Figure1 A-I) or rearrange coloration patterns (Supplementary Figure1 J-L). A draft leopard gecko genome assembly has been published, containing 2.02 Gb of sequence in 22,548 scaffolds, with 24,755 annotated protein-coding genes[1]. Embryonic development *in ovo* and blastema-based tail regeneration have also been staged and documented in great detail[31-33]. Here, we took advantage of these established resources and used quantitative genetics to gain insight into the molecular regulation of white color in leopard geckos.

Results

The Lemon Frost allele is a spontaneous semidominant mutation

A spontaneous mutation occurred in a female hatchling from a cross between two wildtype leopard geckos. This mutation increased the white color of the leopard gecko, resulting in brightened white and yellow colors. This unique color morph was named Lemon Frost[34] (Figure 1). A male leopard gecko carrying the *lemon frost* (*lf*) allele, Mr. Frosty (Figure 1B), was crossed to 12 female leopard geckos of different genetic backgrounds. The F1 progeny, which were heterozygous for the *lf* allele, were backcrossed to the same maternal lines or intercrossed to establish a colony of more than 900 animals (Supplementary Figure 2). Homozygous F2 intercross progeny were named super Lemon Frost (Figure 1C). These homozygous mutants have an accentuated color phenotype and thickened skin, which is most apparent in their eyelids (Figure 1C, red arrow). Heterozygous Lemon Frost animals were also crossed to another mutant, Blizzard, which is light yellow without other colors or patterns (Figure 1D). The homozygous Blizzard progeny carrying the *lf* allele displayed excessive white color in their heads and trunks, which brightened Blizzard's yellow color (Figure 1E). The *lf* allele also increased white color in the retina (Figure 1E). The segregation pattern of Lemon Frost in

pedigrees is consistent with single-locus Mendelian inheritance (Figure 1F-H). The *lf* allele is semidominant, as homozygous mutants have more pronounced phenotypes than do heterozygotes (Figure 1B-C and F-H).

The *lemon frost* allele leads to iridophoroma, with potential metastasis in homozygous animals

Heterozygous Lemon Frost mutants were recently reported to develop iridophoroma[34], a tumor of iridophores. Histopathological examination of the skin samples from homozygous mutants, with accentuated phenotypes, showed large solid sheaths of round to polygonal neoplastic cells that efface and expand the normal tissue architecture (Supplementary Figure 3). The cells have abundant cytoplasm with bright brownish intracytoplasmic pigment. The nuclei are eccentric and vary from round to fusiform. The white tumor masses stain dark with Hematoxylin and Eosin (H&E), and remain brightly reflective under dark-field illumination (Supplementary Figure 4A,B), consistent with their nature as iridophores[26,35-38]. Imaging with Transmission Electron Microscopy (TEM) showed that the *lf* allele led to both increased numbers of neoplastic iridophores and increased production of reflective platelets within each iridophore[39] (Supplementary Figure 4C). In addition to skin, other affected organs in homozygous mutants include liver, eye, and muscle. The interpretation of the widespread neoplastic nodules is that the tumors are malignant iridophoroma.

More than 80% of both male and female animals carrying the *lf* allele developed white tumors 6 months to 5 years after birth. The tumors manifest as patches of white cells in the skin, which are most evident on the ventral side of the animal (Figure 2A). The tumor skin can be severely thickened and leathery (Figure 2B, Supplementary Figure 3). It is resistant to liquid nitrogen freezing, or to Dounce homogenization, making RNA extraction infeasible. In severe cases in

heterozygous mutants, the tumors develop into skin protrusions (Figure 2C, left), which contain dense white masses (Figure 2C, right). Tumors cover a greater fraction of the skin of homozygous mutants. Surprisingly, these tumors rarely develop into skin protrusions as in heterozygous animals. Instead, they manifest as well-demarcated, white, thickened patches on the ventral skin (Figure 2A), thickened layers of white masses all over the dorsal skin (Figure 2B), white, multifocal, variably sized, well-demarcated nodules in the liver, and patches of white cells in the oral cavity (Figure 2D).

Linkage and association analysis in a breeding pedigree

To identify the genetic locus that regulates white color and tumor growth in *Lemon Frost* mutants, we used restriction site-associated DNA sequencing (RAD-Seq) to genotype 188 animals from the breeding pedigree (Figure 3, Supplementary Figure 2), including 33 super Lemon Frost (*lf*/*lf*), 116 Lemon Frost (*lf*/+), and 39 wild-type (+/+) individuals. We identified a total of 14,857 variants covering 2,595 scaffolds of the genome assembly. To map the Lemon Frost locus, we tested the effect of allelic dosage at each marker on white coloration of the geckos in a standard semi-dominant association mapping framework, accounting for population structure through the use of marker-based relatedness. We used a p-value threshold of 7.09e-5 (Methods) to control the false positive rate at 1%. Forty-eight markers on 31 scaffolds were significantly associated with white coloration (Supplemental Table). The top two association signals corresponded to scaffolds 6052 and 996.

Synteny analysis and homozygosity mapping

Because the gecko genome assembly is highly fragmented, we used synteny to examine whether the 31 scaffolds associated with coloration belong to a single genomic interval. We compared the gecko scaffolds to homologous regions of the most closely related species with chromosome-scale genome assemblies: chicken[40] and human[41]. We found that 17 out of 22

scaffolds that have synteny information (including scaffolds 6052 and 996) correspond to one region on chicken chromosome 5 and human chromosome 15 (Figure 3A-C, Supplemental Table). The 28 markers on these 17 scaffolds are in linkage disequilibrium (Figure 3B), which decays with distance when markers are ordered by synteny (Figure 3B). These results indicate that a single genomic region is associated with the Lemon Frost phenotype, as expected for a new mutation with a Mendelian segregation pattern.

To narrow down the location of the causal gene within this genomic region, we used whole genome sequencing and homozygosity mapping. We pooled DNA from 25 super Lemon Frost genomes (*lf*/*lf*), 63 Lemon Frost genomes (*lf*/+), and 71 wildtype geckos (+/+) and sequenced each pool to 30x coverage. We reasoned that the *lf* mutation in Mr. Frosty and its flanking variants should form a haplotype that would be found in the super Lemon Frost pool with 100% frequency, in the Lemon Frost pool with 50% frequency, and would not be seen in the wildtype pool. We scanned the genome in 10 kb windows and measured the fraction of heterozygous variants from Mr. Frosty that followed this expected pattern in the pools. This statistic was highest for a window on scaffold 996 (Supplementary Table, Methods), the main candidate scaffold from statistical mapping. The expected frequency pattern was observed for 20 of 22 variants in this window (630-640kb on scaffold 996). Four of the top six intervals fall in the region from 570kb to 640kb on scaffold 996, with the signal decaying with distance away from this region (Figure 3D,E). The linkage between this region and Lemon Frost was replicated in an independent 3-generation backcross between Mr. Frosty and a Sunburst Tangerine morph (Figure 4). These results indicate that scaffold 996 contains the Lemon Frost mutation.

SPINT1 is a strong candidate gene for the Lemon Frost phenotype

The genomic interval spanning positions 570kb-640kb on scaffold 996 contains a single gene, SPINT1. SPINT1 (serine peptidase inhibitor, Kunitz type 1), also known as hepatocyte growth

156 factor activator inhibitor type 1 (HAI-1), is a transmembrane serine protease inhibitor expressed
157 mainly in epithelial cells[2,3,16]. It is the only gene in the larger associated region reported to be a
158 suppressor of epithelial cell tumors in model organisms and in humans[2,4-14,42]. Because the
159 breeding and transmission data indicate that the *lf* allele arose from a single spontaneous
160 mutation, we reasoned that a mutation disrupting SPINT1 causes the over-proliferation of white-
161 colored skin cells in Lemon Frost geckos.
162
163 The Lemon Frost SPINT1 allele differs from the reference genome assembly at two positions in
164 the exons, as well as at 147 positions in the introns and the 3'UTR (Supplemental Table). This
165 large number of variants is a consequence of differences in genetic background between Mr.
166 Frosty's parents and the non-Lemon Frost individual used to generate the reference, and makes
167 it challenging to identify the causal mutation. Both differences in the coding sequence of
168 SPINT1 are synonymous. Notable differences in non-coding regions include 7 large
169 insertion/deletions (indels) in the introns and a 13-nucleotide insertion in the 3'UTR
170 (CAAGTGTATGTAT). Indels in introns and promoters of SPINT1 have been reported to lead to
171 loss of SPINT1 function in fish and mice[8,9,6].
172
173 Sequencing of RNA extracted from normal gecko skin and from skin peripheral to tumors in
174 homozygous mutants confirmed that SPINT1 is expressed in this tissue (Supplemental Figure
175 5). However, we did not observe a significant difference between homozygous mutants and
176 wildtype geckos in SPINT1 mRNA levels or splicing patterns. This result suggests that the
177 putative causal mutation in SPINT1 may alter translation or protein activity, rather than
178 transcription. Alternatively, the mutation might reduce SPINT1 expression only in tumors, which
179 are refractory to RNA extraction as noted above.
180
181 **Discussion**

Several lines of evidence support our hypothesis that a defect in SPINT1 causes iridophoroma in Lemon Frost geckos. First, SPINT1 function is dosage-dependent, consistent with our observation that Lemon Frost is a semi-dominant phenotype. In humans, carcinoma tissues *in vivo* and carcinoma-derived cell lines *in vitro* have reduced SPINT1 on the cell membrane[15,43] through enhanced shedding of the extracellular domain or decreased mRNA or protein expression. Reduced expression of SPINT1 has been associated with a negative prognosis of human Skin Cutaneous Melanoma (SKCM)[4] and pancreatic ductal adenocarcinoma[13]. Knockdown of SPINT1 expression by siRNA in cancer cell lines led to increased invasion or metastasis[14,15,44]. Second, loss of SPINT1 function in fish and mice leads to tumor formation in epithelial cells. In mice, homozygous deletion of SPINT1 leads to disrupted placental basement membranes and embryonic lethality[9,11]. Rescued mosaic animals developed scaly skin with hyperkeratinization[12]. Intestine-specific deletion of SPINT1 leads to increased tumor growth of intestine epithelium[10]. Increased expression of SPINT1 in the skin abrogated matriptase-induced spontaneous skin squamous cell carcinoma[45]. In zebrafish, reduced expression led to hyperproliferation of basal keratinocytes[8] and enhanced proliferation of epithelial cells[6]. Furthermore, SPINT1 deficiency was used to establish a disease model for Skin Cutaneous Melanoma (SKCM) in zebrafish[4]. In all three studies in zebrafish, skin inflammation was observed. Third, insertions in introns[8,9] and promoters[6] have caused loss of SPINT1 function. Together with our genetic localization of the *lf* locus to SPINT1, these lines of evidence make this gene a very strong candidate for the Lemon Frost phenotype.

Molecular genetics in reptiles is not well established due to long reproductive cycles and challenges in laboratory breeding. Early work focused on careful documentation of patterns of inheritance[18,46]. Molecular studies have examined sequence variants in a candidate pigmentation gene, melanocortin-1 receptor, and their association with melanic or blanched phenotypes in different species and ecological niches[47-54]. Recently, CRISPR-Cas9-mediated

gene editing was successfully used to mutate the tyrosinase gene in the lizard *Anolis sagrei*[55]. Although this species is only distantly related to the leopard gecko, this advance offers promise that targeted studies of the role of SPINT1 mutations in the Lemon Frost phenotype will become possible.

White iridophoroma is common in many reptile species[56], including green iguanas[57], captive snakes[58], bearded dragons[59] and veiled chameleons[60]. The genetic causes of this phenotype in these species are unknown. Most of our knowledge about molecular and cellular regulation of iridophores derives from work in zebrafish[27-29,61-71]. Interestingly, few cases of iridophoroma have been reported in zebrafish[72]. We found that an evolutionarily conserved gene, SPINT1, regulates the proliferation of white iridophores in the leopard gecko. The tumor suppressor function of SPINT1 establishes a link between iridophoroma and regulation of white coloration in reptiles. Our work suggests that cancer genes can play as important a role in iridophores as they do in melanocytes and melanoma[73], and that Lemon Frost leopard geckos can serve as a disease model to study Skin Cutaneous Melanoma.

Methods

Gecko maintenance and experimental procedures

All activities involving animals included in this manuscript were approved by the University of California, Los Angeles (UCLA) Institutional Animal Care and Use Committee. Leopard geckos were acquired from a commercial breeder. Housing conditions at UCLA included: room temperature of 70-80 F, cage temperature of 72-95 F, room relative humidity between 30-60%, and a 12:12 hours light cycle. A heating pad was provided at one side of the cage to establish a temperature gradient. Animals were singly housed in polycarbonate cages with cardboard lines

(Techboard®) at the bottom, water was provided in bowls inside the cage, and PVC pipe pieces and plastic plants were offered as environmental enrichment. Geckos were fed 2-6 fresh crickets and 2-4 mealworms three times per week.

Geckos were euthanized with an intracoelomic injection of sodium pentobarbital (Euthasol®) at a dose of 100-200 mg/Kg. Immediately after euthanasia, a necropsy was performed, including external examination, body and organ weighing, gross assessment of normal and abnormal tissues, and tissue collection for histopathology processing and assessment. Normal and abnormal tissues were fixed in 10% formalin, embedded in paraffin, sectioned, and stained with H&E for pathologic evaluation.

Phenotyping

Lemon Frost and super Lemon Frost phenotypes were determined according to a list of rules, based on increased white color of the body, eye, and belly compared to normal wildtype animals (http://www.geckosetc.com/lemon_frost_info.html). Pictures were taken for each animal to document the phenotype.

Genotyping

Genomic DNA was extracted from fresh tail tips with Easy-DNA gDNA purification kit (K180001, ThermoFisher), or from the saliva with PERFORMAgene (PG-100, DNAgenotek). Genomic DNA extracted from saliva was further purified with ethanol precipitation before genotyping assays. DNA libraries for whole genome sequencing were prepared with Nextera DNA Library Prep Kit (FC-121-1031, Illumina). Libraries for RADseq were prepared according to the

259 procedures of Adapterama III[74] with few modifications. Libraries were sequenced on a HiSeq
260 3000 (Illumina).
261
262 Only scaffolds larger than 5kb in the draft genome assembly were used as a reference. RADseq
263 reads and Whole Genome Sequencing (WGS) reads were aligned to the leopard gecko draft
264 genome[1] with bwa mem[75]. Variants for WGS were identified with GATK[76]. Variants for RADseq
265 were identified with Stacks[77,78]. All variants were filtered with VCFtools[79]. Only high-quality
266 variants were used in homozygosity mapping or statistical mapping (DP>=30, GQ>=30).
267
268 Transcriptome sequencing
269
270 Skin tissue samples around 6mm in diameter were taken from the ventral side of the geckos
271 after anesthetization with 1-5% isoflurane. As tumor tissues are refractory to RNA extraction,
272 flanking tumor-free tissue samples were taken for homozygous Lemon Frost animals. All
273 samples were homogenized with TissueRuptor in buffer RLT immediately after collection.
274 Lysates were immediately frozen on dry ice until all tissues were collected from animals. Then
275 all lysates were centrifuged for 5 minutes at 13,000 rpm to remove debris. Supernatants were
276 taken to fresh tubes, and mRNA was extracted according to the procedures of RNeasy Fibrous
277 Tissue Mini Kit (74704, QIAGEN).
278
279 Libraries of extracted mRNA were prepared with RNA HyperPrep kit (KAPA) and sequenced on
280 a HiSeq 3000 (Illumina). RNA-seq reads were mapped to the leopard gecko draft genome[1]
281 using HISAT2 with default parameters. Identification of alternative and differential splicing
282 events was performed using JuncBase[80]. Gene expression was compared using Sleuth[81] after
283 RNA transcript abundance was quantified using Kallisto[82].
284

Pathology

Complete postmortem examination was performed, and representative tissue samples were obtained. All tissues obtained at necropsy were preserved in 10% neutral-buffered formalin solution for up to 5 days before being processed and embedded in paraffin. All tissues were sectioned at 5 µm, and routinely stained with Hematoxylin and Eosin.

Statistical Mapping

Biallelic markers with minor allele frequency of less than 5% and with fewer than 10 individuals called as homozygous for both the reference and alternative alleles were excluded from mapping and kinship matrix construction. A kinship matrix was calculated using the function *A.mat* with default parameters from the rrBLUP[83] R package. Phenotype was encoded as 0 for wild type, 1 for Lemon Frost, and 2 for super Lemon Frost. Association statistics between this phenotype vector and marker genotypes were computed using the function *gwas2* in the NAM[84] R package using a linear mixed model with a random effect of kinship to control for population structure. The effective number of tests was computed to be 141.1 based on the procedure of Galwey et al[85]. A family-wise error rate significance threshold was calculated as 0.01/141.1 or p<7.09e-5.

Homozygosity Mapping

Pooled animals and Mr. Frosty were sequenced to ~30x coverage on a HiSeq 3000 (Illumina). Variants were identified with GATK and filtered with VCFtools. Biallelic heterozygous variants from Mr. Frosty, including indels, were used as markers to localize the Lemon Frost mutation. Allele ratios (AF) were calculated by dividing the read count of alternative alleles by the sum of

the counts of reference alleles and alternative alleles. Variants closely linked to the Lemon Frost mutation are expected to have AF between 0.4 and 0.6 in the Lemon Frost pool and in Mr. Frosty, AF > 0.85 in the super Lemon Frost pool, and AF < 0.15 in the wildtype pool. The number of variants meeting these criteria was counted for every 10kb genome interval. The fraction of such variants among all variants heterozygous in Mr. Frosty within the interval was then calculated. Intervals with fewer than 5 variants were excluded because they could not provide statistically meaningful results.

Transmission Electron Microscopy

Dissected skin tissues were fixed in 2.5% glutaraldehyde and 4% formaldehyde in 0.1 M sodium cacodylate buffer overnight at 4 °C. After being washed in PBS, samples were post-fixed in 1% osmium tetroxide in 0.1M sodium cacodylate, and dehydrated through a graded series of ethanol concentrations. After infiltration with Eponate 12 resin, the samples were embedded in fresh Eponate 12 resin and polymerized at 60°C for 48 hours. Ultrathin sections of 70 nm thickness were prepared, placed on formvar-coated copper grids, and stained with uranyl acetate and Reynolds' lead citrate. The grids were examined using a JEOL 100CX transmission electron microscope at 60 kV, and images were captured by an AMT digital camera (Advanced Microscopy Techniques Corporation, model XR611).

Acknowledgement

We thank Aaron Miller, Jasmine Gonzalez, Kendall Placido and James Walter for their assistance in gecko DNA collection and phenotyping. We thank members of the Kruglyak lab for helpful feedbacks on the project, and Giancarlo Bruni, Stefan Zdraljevic, Eyal Ben-David and Olga Schubert for helpful comments on the manuscript. We thank Chunni Zhu (Electron

Microscopy Core Facility, UCLA Brain Research Institute) for her assistance in TEM sample processing and imaging. We thank Jonathan Eggenschwiler for helpful discussions.

This work is supported by the Howard Hughes Medical Institute (LK) and the Helen Hay Whitney Foundation (LG).

Figure legends

Fig 1 The Lemon Frost mutant of the common leopard gecko, *Eublepharis macularius*. (A) wild type; (B) heterozygous mutant; (C) homozygous mutant, with red arrow pointing to the eye lid; (D) blizzard mutant with minimal color; (E) Lemon Frost mutation (*lf*) on the blizzard background; (F-H) segregation of the *lf* allele. Lemon Frost (LF) denotes heterozygotes for the mutation; super LF denotes homozygotes for the mutation. All proportions are consistent with expectations for single-locus Mendelian inheritance (chi-square test $p > 0.1$).

Fig 2 Tumor growth and metastasis in the Lemon Frost mutant. Designations are homozygous mutant (*lf*/*lf*); heterozygous mutant (*lf*/+); wild type (+/+). (A) tumors in ventral skin; (B) thick layers of white tumor cells (*lf*/*lf*) vs. normal white cells (+/+); (C) outgrowth of white tumor cells (*lf*/+); (D) metastasis of white tumor cells in the liver and oral cavity. Red arrows: white colored tumor cells. Arrowhead in B: normal white cells.

Fig 3 Localization of the Lemon Frost mutation. (A) p-value for association with white color and (B) linkage disequilibrium for 28 markers syntenic to chicken chromosome 15 (red, ordered by synteny), 4 markers syntenic to chromosome 5 (cyan), and 16 markers without synteny information (green). (C) A schematic of the region showing synteny and gene annotation. (D) Fraction of markers showing expected allele frequency pattern in pools, plotted for 10kb windows along scaffold 996. The four windows with the highest fraction are marked by asterisks and span the location of the gene SPINT1. Windows with fewer than 5 variants were not plotted (dashed red lines). (E) Genome-wide distribution of the fraction of markers showing expected allele frequency pattern in pools for all 10 kb windows. The 4 highest windows on scaffold 996 (red arrows) marked in D are among the 6 highest windows in the entire genome.

Fig 4 The *lemon frost* allele in a backcross. (A) We genotyped 7 progeny with the Lemon Frost phenotype and 6 wild type progeny from the third generation of a backcross of Mr. Frosty to the Sunburst line for markers in the SPINT1 region and observed a consistent inheritance pattern. (B) Sequencing chromatogram of a heterozygous animal (*lf*/+) at an insertion marker. (C) Sequencing chromatogram of a homozygous animal (+/+) at the same insertion marker.

SupFig 1 Coloration and pattern diversity of the common leopard gecko, *Eublepharis macularius*. (A) wild type; (B) black night; (C) variant of black night; (D) granite snow; (E) gem snow; (F) white knight; (G) sunburst tangerine; (H-I) variants of sunburst tangerine; (J) red stripes; (K) bold stripes; (L) rainbow.

SupFig 2 Breeding pedigree of the Lemon Frost mutation. Mr. Frosty, the original carrier of the spontaneous Lemon Frost mutation, was bred to 12 female geckos from different genetic

backgrounds. F1s carrying the *lf* allele were bred among themselves or back to their female parent, producing the second generation of animals heterozygous or homozygous for the *lf* allele. Blue: *lf*/*lf*; green: *lf*/+; red:+/+. Dashed line: same individual/line.

SupFig 3 Histopathology of skin tumors. (A) Thick layers of white tumor tissue (star) infiltrating white skin (arrow). (B) Skin biopsies organized and fixed in a paper roll for sectioning. (C) H&E staining of the skin sections. Arrow: skin; star: infiltrated tumor mass. (D) H&E staining of the skin sections showing normal skin cells and neoplastic cells (star). Neoplastic cells have eccentric and condensed nuclei.

SupFig 4 Potential metastasis of iridophoroma. (A) In normal skin, cell nuclei are oval and perpendicular to the skin surface. In Lemon Frost skin, cell nuclei are flat, elongated and parallel to the skin, reminiscent of epithelial-to-mesenchymal transition. (B) Iridophoroma in the liver, stained dark in H&E sections. In dark field imaging, iridophores are bright white. Such iridophores invade blood vessels in the tissue (red arrows). (C) In TEM imaging, white tumor skins in super LF are filled with abundant iridophores with excessive brightly reflective crystals (Tumor). In normal skin, iridophores are much fewer and have less crystals (Normal).

SupFig 5 SPINT1 expression in gecko skin. SPINT1 mRNA reads from transcriptome sequencing were aligned to the genome and visualized in IGV. Top 3 rows show samples from homozygous mutants. Bottom 3 rows show samples from wild type geckos. Skin tissue adjacent to the tumors was used in the mutants. Peaks mark SPINT1 exons. The last exon on the right is transcribed together with the 3'UTR.

References

1 Xiong, Z. *et al.* Draft genome of the leopard gecko, Eublepharis macularius. *GigaScience* **5**, doi:10.1186/s13742-016-0151-4 (2016).

2 Kataoka, H., Kawaguchi, M., Fukushima, T. & Shimomura, T. Hepatocyte growth factor activator inhibitors (HAI-1 and HAI-2): Emerging key players in epithelial integrity and cancer. *Pathol Int* **68**, 145-158, doi:10.1111/pin.12647 (2018).

3 Shimomura, T. *et al.* Hepatocyte growth factor activator inhibitor, a novel Kunitz-type serine protease inhibitor. *J Biol Chem* **272**, 6370-6376, doi:10.1074/jbc.272.10.6370 (1997).

4 Gomez-Abenza, E. *et al.* Zebrafish modeling reveals that SPINT1 regulates the aggressiveness of skin cutaneous melanoma and its crosstalk with tumor immune microenvironment. *J Exp Clin Cancer Res* **38**, 405, doi:10.1186/s13046-019-1389-3 (2019).

5 Kawaguchi, M. *et al.* Membrane-bound serine protease inhibitor HAI-1 is required for maintenance of intestinal epithelial integrity. *Am J Pathol* **179**, 1815-1826, doi:10.1016/j.ajpath.2011.06.038 (2011).

6 Mathias, J. R. *et al.* Live imaging of chronic inflammation caused by mutation of zebrafish Hai1. *J Cell Sci* **120**, 3372-3383, doi:10.1242/jcs.009159 (2007).

7 Kawaguchi, M. *et al.* Inhibition of nuclear factor-kappaB signaling suppresses Spint1-deletion-induced tumor susceptibility in the ApcMin/+ model. *Oncotarget* **7**, 68614-68622, doi:10.18632/oncotarget.11863 (2016).

8 Carney, T. J. *et al.* Inactivation of serine protease Matriptase1a by its inhibitor Hai1 is required for epithelial integrity of the zebrafish epidermis. *Development* **134**, 3461-3471, doi:10.1242/dev.004556 (2007).

9 Fan, B. *et al.* Hepatocyte growth factor activator inhibitor-1 (HAI-1) is essential for the integrity of basement membranes in the developing placental labyrinth. *Dev Biol* **303**, 222-230, doi:10.1016/j.ydbio.2006.11.005 (2007).

10 Hoshiko, S. *et al.* Hepatocyte growth factor activator inhibitor type 1 is a suppressor of intestinal tumorigenesis. *Cancer Res* **73**, 2659-2670, doi:10.1158/0008-5472.CAN-12-3337 (2013).

11 Tanaka, H. *et al.* Hepatocyte growth factor activator inhibitor type 1 (HAI-1) is required for branching morphogenesis in the chorioallantoic placenta. *Mol Cell Biol* **25**, 5687-5698, doi:10.1128/MCB.25.13.5687-5698.2005 (2005).

12 Nagaike, K. *et al.* Defect of hepatocyte growth factor activator inhibitor type 1/serine protease inhibitor, Kunitz type 1 (Hai-1/Spint1) leads to ichthyosis-like condition and abnormal hair development in mice. *Am J Pathol* **173**, 1464-1475, doi:10.2353/ajpath.2008.071142 (2008).

13 Sakugawa, C. *et al.* Prognostic significance of hepatocyte growth factor activator inhibitor type 1 (HAI-1) immunoreactivity in pancreatic ductal adenocarcinoma. *BMC Res Notes* **10**, 674, doi:10.1186/s13104-017-3014-x (2017).

14 Baba, T. *et al.* Loss of membrane-bound serine protease inhibitor HAI-1 induces oral squamous cell carcinoma cells' invasiveness. *J Pathol* **228**, 181-192, doi:10.1002/path.3993 (2012).

15 Ye, J. *et al.* Loss of hepatocyte growth factor activator inhibitor type 1 participates in metastatic spreading of human pancreatic cancer cells in a mouse orthotopic transplantation model. *Cancer Sci* **105**, 44-51, doi:10.1111/cas.12306 (2014).

16 Kataoka, H. *et al.* Distribution of hepatocyte growth factor activator inhibitor type 1 (HAI-1) in human tissues. Cellular surface localization of HAI-1 in simple columnar epithelium and its modulated expression in injured and regenerative tissues. *J Histochem Cytochem* **47**, 673-682, doi:10.1177/002215549904700509 (1999).

17 Fujii, R. in *International Review of Cytology* Vol. 143 (eds Kwang W. Jeon, Martin Friedlander, & Jonathan Jarvik) 191-255 (Academic Press, 1993).

18 Olsson, M., Stuart-Fox, D. & Ballen, C. Genetics and evolution of colour patterns in reptiles. *Seminars in Cell & Developmental Biology* **24**, 529-541, doi: 10.1016/j.semcdb.2013.04.001 (2013).

19 Cuthill, I. C. *et al.* The biology of color. *Science* **357**, doi:10.1126/science.aan0221 (2017).

20 Shawkey, M. D. & D'Alba, L. Interactions between colour-producing mechanisms and their effects on the integumentary colour palette. *Philos Trans R Soc Lond B Biol Sci* **372**, doi:10.1098/rstb.2016.0536 (2017).

21 Thayer, R. C., Allen, F. I. & Patel, N. H. Structural color in Junonia butterflies evolves by tuning scale lamina thickness. *Elife* **9**, doi:10.7554/eLife.52187 (2020).

22 Kelsh, R. N., Harris, M. L., Colanesi, S. & Erickson, C. A. Stripes and belly-spots -- a review of pigment cell morphogenesis in vertebrates. *Semin Cell Dev Biol* **20**, 90-104, doi:10.1016/j.semcdb.2008.10.001 (2009).

23 Parichy, D. M. & Spiewak, J. E. Origins of adult pigmentation: diversity in pigment stem cell lineages and implications for pattern evolution. *Pigment Cell Melanoma Res* **28**, 31-50, doi:10.1111/pcmr.12332 (2015).

24 Nordlund, J. J., Abdel-Malek, Z. A., Boissy, R. E. & Rheins, L. A. Pigment Cell Biology: An Historical Review. *Journal of Investigative Dermatology* **92**, S53-S60, doi: 10.1038/jid.1989.33 (1989).

25 Nordlund, J. J. *et al. The Pigmentary System: Physiology and Pathophysiology*. 2nd edn, (Wiley, 2008).

26 Goda, M. & Fujii, R. The Blue Coloration of the Common Surgeonfish, Paracanthurus hepatus-II. Color Revelation and Color Changes. *Zoolog Sci* **15**, 323-333, doi:10.2108/zsj.15.323 (1998).

27 Frohnhofer, H. G., Krauss, J., Maischein, H. M. & Nusslein-Volhard, C. Iridophores and their interactions with other chromatophores are required for stripe formation in zebrafish. *Development* **140**, 2997-3007, doi:10.1242/dev.096719 (2013).

28 Salis, P. *et al.* Developmental and comparative transcriptomic identification of iridophore contribution to white barring in clownfish. *Pigment Cell Melanoma Res* **32**, 391-402, doi:10.1111/pcmr.12766 (2019).

29 Krauss, J. *et al.* Endothelin signalling in iridophore development and stripe pattern formation of zebrafish. *Biol Open* **3**, 503-509, doi:10.1242/bio.20148441 (2014).

30 Kaelin, C. B. *et al.* Specifying and sustaining pigmentation patterns in domestic and wild cats. *Science* **337**, 1536-1541, doi:10.1126/science.1220893 (2012).

31 Wise, P. A. D., Vickaryous, M. K. & Russell, A. P. An Embryonic Staging Table for In Ovo Development of Eublepharis macularius, the Leopard Gecko. *The Anatomical Record* **292**, 1198-1212, doi:10.1002/ar.20945 (2009).

32 McLean, K. E. & Vickaryous, M. K. A novel amniote model of epimorphic regeneration: the leopard gecko, Eublepharis macularius. *BMC Developmental Biology* **11**, 50, doi:10.1186/1471-213X-11-50 (2011).

33 Delorme, S. L., Lungu, I. M. & Vickaryous, M. K. Scar-Free Wound Healing and Regeneration Following Tail Loss in the Leopard Gecko, Eublepharis macularius. *The Anatomical Record* **295**, 1575-1595, doi:10.1002/ar.22490 (2012).

34 Szydłowski, P. *et al.* Iridophoroma associated with the Lemon Frost colour morph of the leopard gecko (Eublepharis macularius). *Scientific Reports* **10**, 5734, doi:10.1038/s41598-020-62828-9 (2020).

35 Bagnara, J. T. in *International Review of Cytology* Vol. 20 (eds G. H. Bourne & J. F. Danielli) 173-205 (Academic Press, 1966).

36 Denefle, J. P. & Lechaire, J. P. Localization of pigment cells in cultured frog skin. *Am J Anat* **188**, 212-220, doi:10.1002/aja.1001880210 (1990).

37 DeMartini, D. G., Krogstad, D. V. & Morse, D. E. Membrane invaginations facilitate reversible water flux driving tunable iridescence in a dynamic biophotonic system. *Proc Natl Acad Sci U S A* **110**, 2552-2556, doi:10.1073/pnas.1217260110 (2013).

38 Aramaki, T. & Kondo, S. Method for disarranging the pigment pattern of zebrafish by optogenetics. *Developmental Biology* **460**, 12-19, doi: 10.1016/j.ydbio.2018.12.019 (2020).

514 39 Morrison, R. L. & Frost-Mason, S. K. Ultrastructural analysis of iridophore
515 organellogenesis in a lizard, Sceloporus graciosus (Reptilia: Phrynosomatidae). *J Morphol*
516 **209**, 229-239, doi:10.1002/jmor.1052090209 (1991).
517 40 Hillier, L. W. *et al.* Sequence and comparative analysis of the chicken genome provide
518 unique perspectives on vertebrate evolution. *Nature* **432**, 695-716,
519 doi:10.1038/nature03154 (2004).
520 41 Lander, E. S. *et al.* Initial sequencing and analysis of the human genome. *Nature* **409**,
521 860-921, doi:10.1038/35057062 (2001).
522 42 Cheng, H., Fukushima, T., Takahashi, N., Tanaka, H. & Kataoka, H. Hepatocyte growth
523 factor activator inhibitor type 1 regulates epithelial to mesenchymal transition through
524 membrane-bound serine proteinases. *Cancer Res* **69**, 1828-1835, doi:10.1158/0008-
525 5472.CAN-08-3728 (2009).
526 43 Kataoka, H. *et al.* Evaluation of hepatocyte growth factor activator inhibitor expression
527 in normal and malignant colonic mucosa. *Cancer Letters* **128**, 219-227, doi:
528 10.1016/S0304-3835(98)00067-6 (1998).
529 44 Koivuniemi, R. *et al.* Hepatocyte growth factor activator inhibitor-1 is induced by bone
530 morphogenetic proteins and regulates proliferation and cell fate of neural progenitor
531 cells. *PLoS One* **8**, e56117, doi:10.1371/journal.pone.0056117 (2013).
532 45 List, K. *et al.* Deregulated matriptase causes ras-independent multistage carcinogenesis
533 and promotes ras-mediated malignant transformation. *Genes Dev* **19**, 1934-1950,
534 doi:10.1101/gad.1300705 (2005).
535 46 Olsson, M. *et al.* Mating system variation and morph fluctuations in a polymorphic lizard.
536 *Molecular Ecology* **16**, 5307-5315, doi: 10.1111/j.1365-294X.2007.03578.x (2007).
537 47 Micheletti, S., Parra, E. & Routman, E. J. Adaptive Color Polymorphism and Unusually
538 High Local Genetic Diversity in the Side-Blotched Lizard, Uta stansburiana. *PLOS ONE* **7**,
539 e47694, doi:10.1371/journal.pone.0047694 (2012).
540 48 Rosenblum, E. B., Hoekstra, H. E. & Nachman, M. W. ADAPTIVE REPTILE COLOR
541 VARIATION AND THE EVOLUTION OF THE MCIR GENE. *Evolution* **58**, 1794-1808, doi:
542 10.1111/j.0014-3820.2004.tb00462.x (2004).
543 49 Nunes, V. L., Miraldo, A., Beaumont, M. A., Butlin, R. K. & Paulo, O. S. Association of
544 Mc1r variants with ecologically relevant phenotypes in the European ocellated lizard,
545 Lacerta lepida. *Journal of Evolutionary Biology* **24**, 2289-2298, doi: 10.1111/j.1420-
546 9101.2011.02359.x (2011).
547 50 Fulgione, D., Lega, C., Trapanese, M. & Buglione, M. Genetic factors implied in melanin-
548 based coloration of the Italian wall lizard. *Journal of Zoology* **296**, 278-285, doi:
549 10.1111/jzo.12242 (2015).
550 51 Rosenblum, E. B., Römpler, H., Schöneberg, T. & Hoekstra, H. E. Molecular and
551 functional basis of phenotypic convergence in white lizards at White Sands. *Proceedings*
552 *of the National Academy of Sciences* **107**, 2113, doi:10.1073/pnas.0911042107 (2010).
553 52 Laurent, S. *et al.* The population genomics of rapid adaptation: disentangling signatures
554 of selection and demography in white sands lizards. *Molecular Ecology* **25**, 306-323, doi:
555 10.1111/mec.13385 (2016).

53 Corso, J., Gonçalves, G. L. & Freitas, T. R. O. d. Sequence variation in the melanocortin-1 receptor (MC1R) pigmentation gene and its role in the cryptic coloration of two South American sand lizards. *Genetics and Molecular Biology* **35**, 81-87 (2012).

54 Jin, Y. *et al.* Dorsal Pigmentation and Its Association with Functional Variation in MC1R in a Lizard from Different Elevations on the Qinghai-Tibetan Plateau. *Genome Biology and Evolution*, doi:10.1093/gbe/evaa225 (2020).

55 Rasys, A. M. *et al.* CRISPR-Cas9 Gene Editing in Lizards through Microinjection of Unfertilized Oocytes. *Cell Rep* **28**, 2288-2292 e2283, doi:10.1016/j.celrep.2019.07.089 (2019).

56 Heckers, K. O., Aupperle, H., Schmidt, V. & Pees, M. Melanophoromas and iridophoromas in reptiles. *J Comp Pathol* **146**, 258-268, doi:10.1016/j.jcpa.2011.07.003 (2012).

57 Rousselet, E. *et al.* Cutaneous iridophoroma in a Green iguana (Iguana iguana). *Vet Clin Pathol* **46**, 625-628, doi:10.1111/vcp.12536 (2017).

58 Munoz-Gutierrez, J. F., Garner, M. M. & Kiupel, M. Cutaneous Chromatophoromas in Captive Snakes. *Vet Pathol* **53**, 1213-1219, doi:10.1177/0300985816644302 (2016).

59 de Brot, S., Sydler, T., Nufer, L. & Ruetten, M. Histologic, Immunohistochemical, and Electron Microscopic Characterization of a Malignant Iridophoroma in a Dwarf Bearded Dragon (Pogona Henrylawsoni). *J Zoo Wildl Med* **46**, 583-587, doi:10.1638/2013-0113.1 (2015).

60 Bronson, E., Pereira, M., Sanchez, C. & Murray, S. Iridophoroma in a Veiled Chameleon, Chamaeleo calyptratus. *Journal of Herpetological Medicine and Surgery* **16**, 58-60, doi:10.5818/1529-9651.16.3.58 (2006).

61 Patterson, L. B. & Parichy, D. M. Interactions with iridophores and the tissue environment required for patterning melanophores and xanthophores during zebrafish adult pigment stripe formation. *PLoS Genet* **9**, e1003561, doi:10.1371/journal.pgen.1003561 (2013).

62 Volkening, A. & Sandstede, B. Iridophores as a source of robustness in zebrafish stripes and variability in Danio patterns. *Nat Commun* **9**, 3231, doi:10.1038/s41467-018-05629-z (2018).

63 Hirata, M., Nakamura, K. & Kondo, S. Pigment cell distributions in different tissues of the zebrafish, with special reference to the striped pigment pattern. *Dev Dyn* **234**, 293-300, doi:10.1002/dvdy.20513 (2005).

64 Hirata, M., Nakamura, K., Kanemaru, T., Shibata, Y. & Kondo, S. Pigment cell organization in the hypodermis of zebrafish. *Dev Dyn* **227**, 497-503, doi:10.1002/dvdy.10334 (2003).

65 Singh, A. P., Schach, U. & Nusslein-Volhard, C. Proliferation, dispersal and patterned aggregation of iridophores in the skin prefigure striped colouration of zebrafish. *Nat Cell Biol* **16**, 607-614, doi:10.1038/ncb2955 (2014).

66 Krauss, J. *et al.* transparent, a gene affecting stripe formation in Zebrafish, encodes the mitochondrial protein Mpv17 that is required for iridophore survival. *Biol Open* **2**, 703-710, doi:10.1242/bio.20135132 (2013).

67 Fadeev, A., Krauss, J., Singh, A. P. & Nusslein-Volhard, C. Zebrafish Leucocyte tyrosine kinase controls iridophore establishment, proliferation and survival. *Pigment Cell Melanoma Res* **29**, 284-296, doi:10.1111/pcmr.12454 (2016).

68 Singh, A. P. & Nusslein-Volhard, C. Zebrafish stripes as a model for vertebrate colour pattern formation. *Curr Biol* **25**, R81-R92, doi:10.1016/j.cub.2014.11.013 (2015).

69 Cooper, C. D. *et al.* Protein Kinase A Signaling Inhibits Iridophore Differentiation in Zebrafish. *J Dev Biol* **6**, doi:10.3390/jdb6040023 (2018).

70 Irion, U. & Nusslein-Volhard, C. The identification of genes involved in the evolution of color patterns in fish. *Curr Opin Genet Dev* **57**, 31-38, doi:10.1016/j.gde.2019.07.002 (2019).

71 Lewis, V. M. *et al.* Fate plasticity and reprogramming in genetically distinct populations of Danio leucophores. *Proc Natl Acad Sci U S A* **116**, 11806-11811, doi:10.1073/pnas.1901021116 (2019).

72 Masahito, P., Ishikawa, T. & Sugano, H. Pigment cells and pigment cell tumors in fish. *J Invest Dermatol* **92**, 266S-270S, doi:10.1111/1523-1747.ep13076602 (1989).

73 Yang, K., Oak, A. S. W., Slominski, R. M., Brozyna, A. A. & Slominski, A. T. Current Molecular Markers of Melanoma and Treatment Targets. *Int J Mol Sci* **21**, doi:10.3390/ijms21103535 (2020).

74 Bayona-Vasquez, N. J. *et al.* Adapterama III: Quadruple-indexed, double/triple-enzyme RADseq libraries (2RAD/3RAD). *PeerJ* **7**, e7724, doi:10.7717/peerj.7724 (2019).

75 Li, H. & Durbin, R. Fast and accurate short read alignment with Burrows-Wheeler transform. *Bioinformatics* **25**, 1754-1760, doi:10.1093/bioinformatics/btp324 (2009).

76 McKenna, A. *et al.* The Genome Analysis Toolkit: a MapReduce framework for analyzing next-generation DNA sequencing data. *Genome Res* **20**, 1297-1303, doi:10.1101/gr.107524.110 (2010).

77 Catchen, J., Hohenlohe, P. A., Bassham, S., Amores, A. & Cresko, W. A. Stacks: an analysis tool set for population genomics. *Mol Ecol* **22**, 3124-3140, doi:10.1111/mec.12354 (2013).

78 Catchen, J. M., Amores, A., Hohenlohe, P., Cresko, W. & Postlethwait, J. H. Stacks: building and genotyping Loci de novo from short-read sequences. *G3 (Bethesda)* **1**, 171-182, doi:10.1534/g3.111.000240 (2011).

79 Danecek, P. *et al.* The variant call format and VCFtools. *Bioinformatics* **27**, 2156-2158, doi:10.1093/bioinformatics/btr330 (2011).

80 Brooks, A. N. *et al.* Conservation of an RNA regulatory map between Drosophila and mammals. *Genome Res* **21**, 193-202, doi:10.1101/gr.108662.110 (2011).

81 Pimentel, H., Bray, N. L., Puente, S., Melsted, P. & Pachter, L. Differential analysis of RNA-seq incorporating quantification uncertainty. *Nat Methods* **14**, 687-690, doi:10.1038/nmeth.4324 (2017).

82 Bray, N. L., Pimentel, H., Melsted, P. & Pachter, L. Near-optimal probabilistic RNA-seq quantification. *Nat Biotechnol* **34**, 525-527, doi:10.1038/nbt.3519 (2016).

83 Endelman, J. B. Ridge Regression and Other Kernels for Genomic Selection with R Package rrBLUP. *The Plant Genome* **4**, 250-255, doi:10.3835/plantgenome2011.08.0024 (2011).

641 84 Xavier, A., Xu, S., Muir, W. M. & Rainey, K. M. NAM: association studies in multiple
642 populations. *Bioinformatics* **31**, 3862-3864, doi:10.1093/bioinformatics/btv448 (2015).
643 85 Galwey, N. W. A new measure of the effective number of tests, a practical tool for
644 comparing families of non-independent significance tests. *Genet Epidemiol* **33**, 559-568,
645 doi:10.1002/gepi.20408 (2009).
646

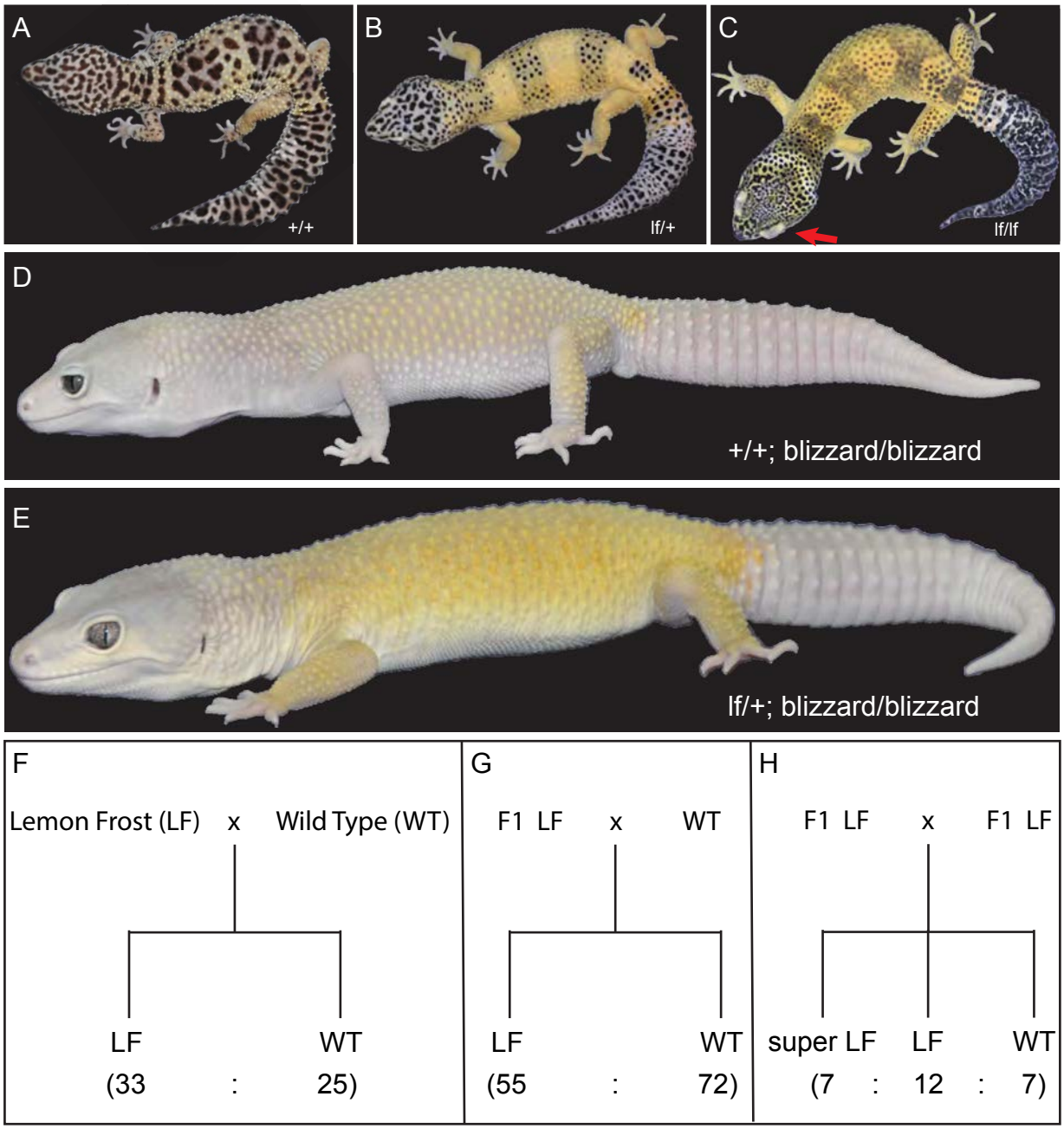

Fig 1 The Lemon Frost mutant of the common leopard gecko, *Eublepharis macularius*. (A) wild type; (B) heterozygous mutant; (C) homozygous mutant, with red arrow pointing to the eye lid; (D) blizzard mutant with minimal color; (E) Lemon Frost mutation (lf) on the blizzard background; (F-H) segregation of the lf allele. Lemon Frost (LF) denotes heterozygotes for the mutation; super LF denotes homozygotes for the mutation. All proportions are consistent with expectations for single-locus Mendelian inheritance (chi-square test $p > 0.1$).

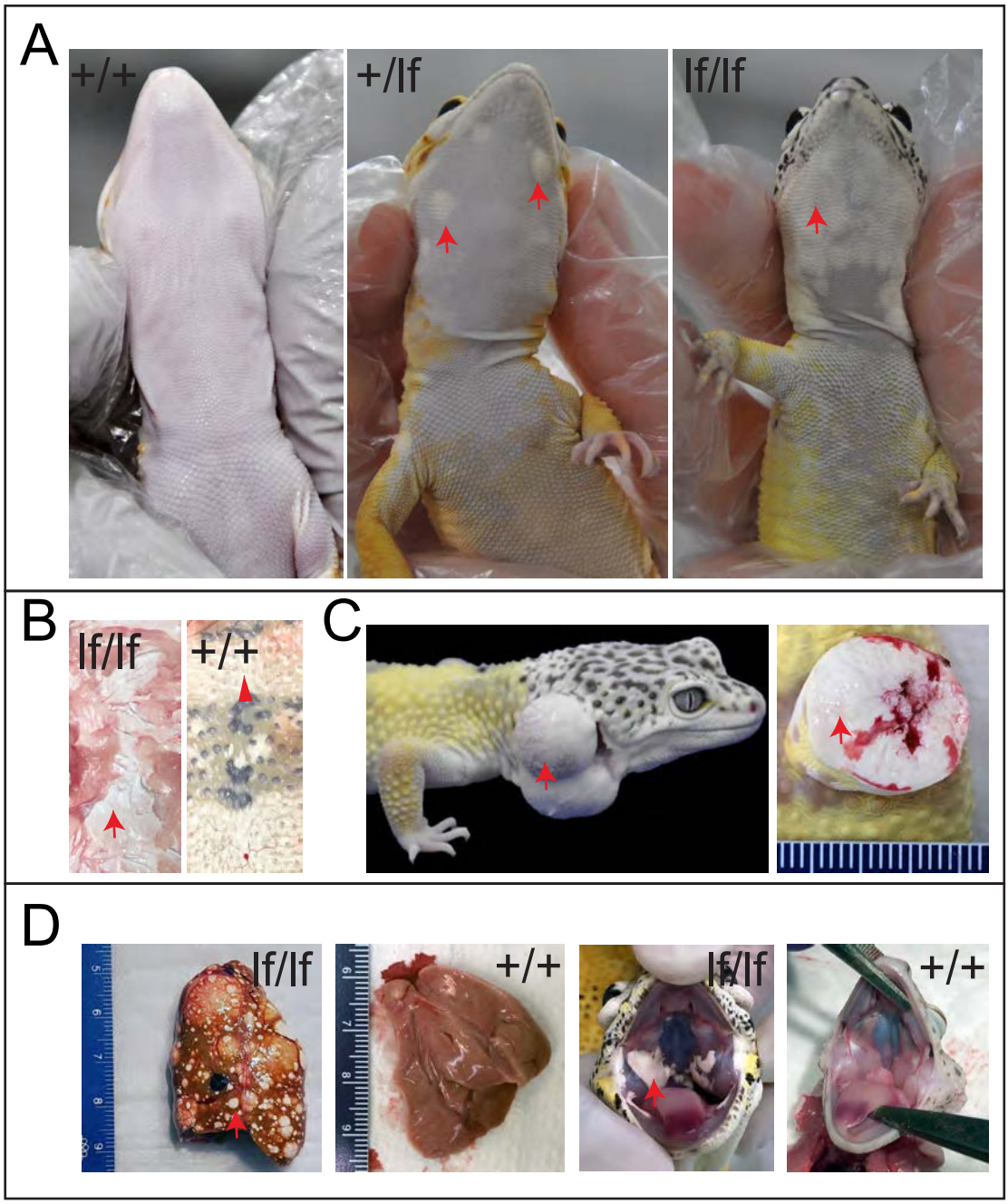

Fig 2 Tumor growth and metastasis in the Lemon Frost mutant. Designations are homozygous mutant (lf/lf); heterozygous mutant (lf); À wild type (+/+). (A) tumors in ventral skin; (B) thick layers of white tumor cells (lf/lf) vs. normal white cells (+/+); (C) outgrowth of white tumor cells (lf/+); (D) metastasis of white tumor cells in the liver and oral cavity. Red arrows: white colored tumor cells. Arrowhead in B: normal white cells.

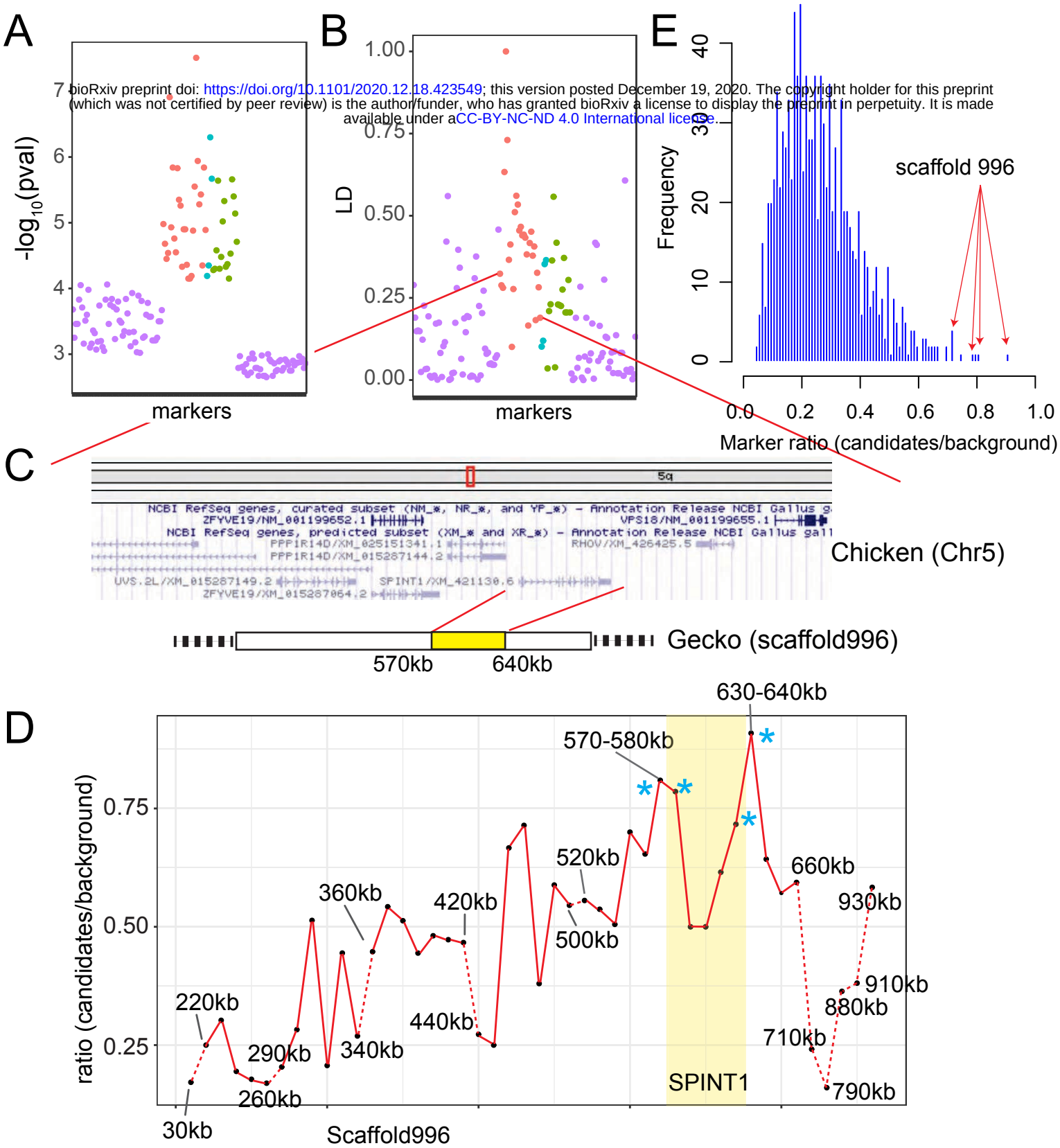

Fig 3 Localization of the Lemon Frost mutation. (A) p-alue for association with white color` and (B) linkage disequilibrium for 28 markers syntenic to chicken chromosome 1 (red, ordered` by synteny), 4 markers syntenic to chromosome 5 (cyan), and 16 markers without synteny information (green). (C) A schematic of the region showing synteny and gene annotation. (D) Fraction of markers showing expected allele frequency pattern in pools, plotted for 10kb windows along scaffold 99. The four windows with the highest fraction` are marked by asterisks and span the location of the gene SPINT1. Windows with fewer than 5 variants were not plotted (dashed red lines). (E) Genome-wide distribution of the fraction of markers showing epected allele` frequency pattern in pools for all 10 kb windows. The 4 highest windows on scaffold 99 (red` arrows) marked in D are among the 6 highest windows in the entire genome.

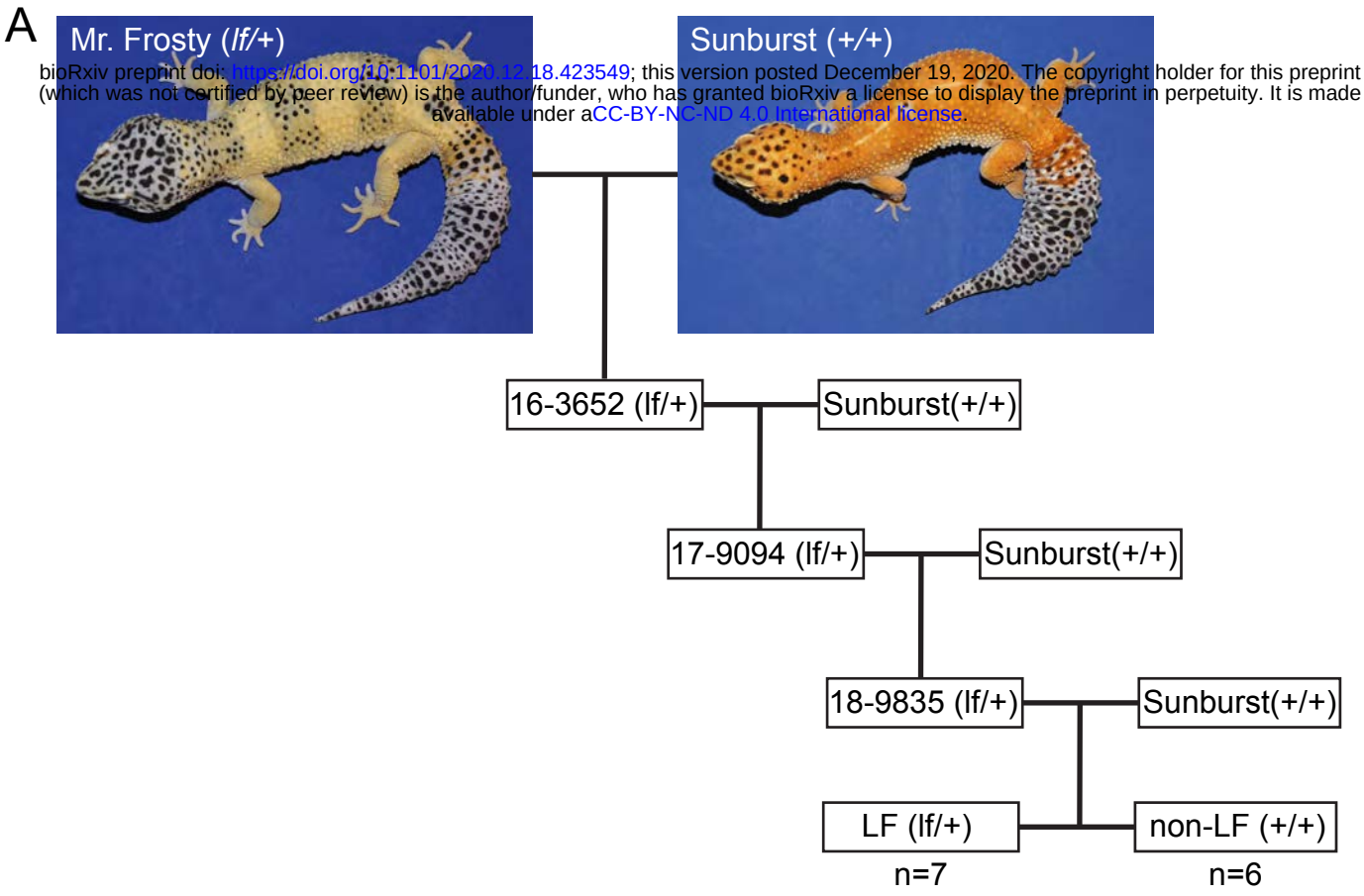

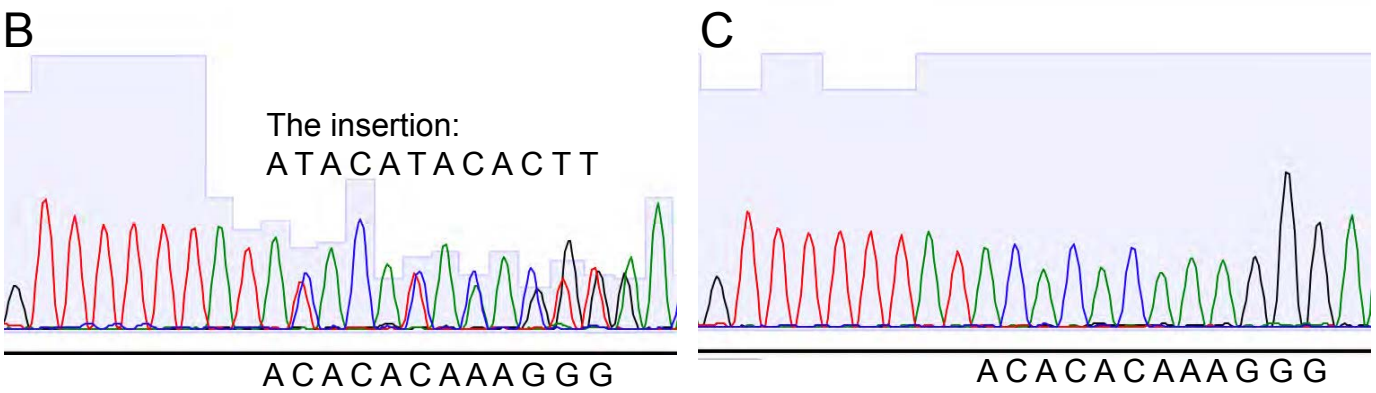

**Fig The` *lemon frost* allele in a backcross.** (A) We genotyped 7 progeny with the Lemon Frost phenotype and 6 wild type progeny from the third generation of a backcross of Mr. Frosty to the Sunburst line for markers in the SPINT1 region and obsered a` consistent inheritance pattern. (B) Sequencing chromatogram of a heterozygous animal (lf/+) at an insertion marker. (C) Sequencing chromatogram of a homozygous animal (+/+) at the same insertion marker.

SupFig 1 Coloration and pattern diversity of the common leopard gecko, *Eublepharis macularius*. (A) wild type; (B) black night; (C) variant of black night; (D) granite snow; (E) gem snow; (F) white knight; (G) sunburst tangerine; (H-I) variants of sunburst tangerine; (J) red stripes; (K) bold stripes; (L) rainbow.

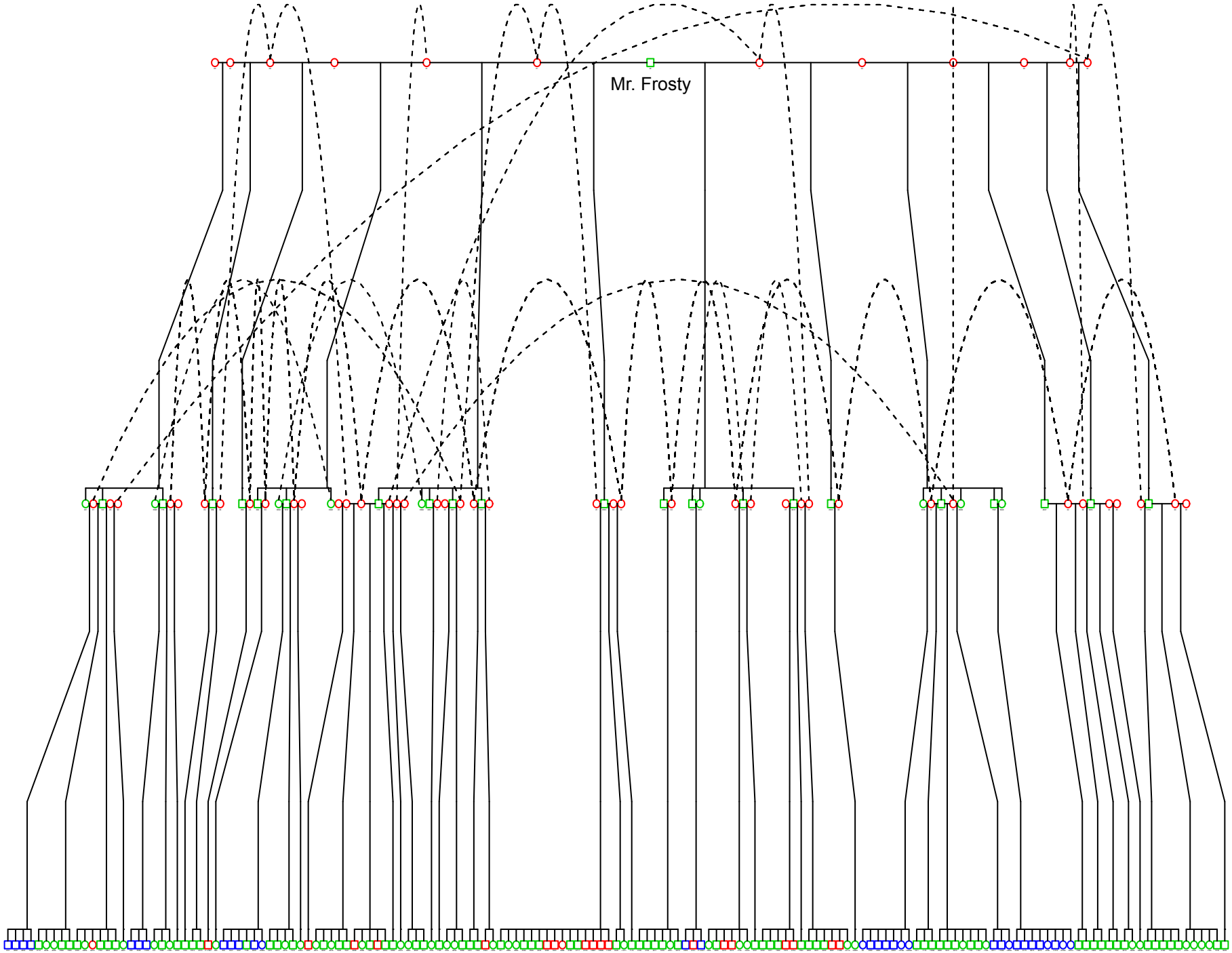

SupFig 2 Breeding pedigree of the Lemon Frost mutation. Mr. Frosty, the original carrier of the spontaneous Lemon Frost mutation, was bred to 12 female geckos from different genetic backgrounds. F1s carrying the lf allele were bred among themselves or back to their female parent, producing the second generation of animals heterozygous or homozygous for the lf allele. Blue: lf/lf; green: lf/+; red:+/+. Dashed line:

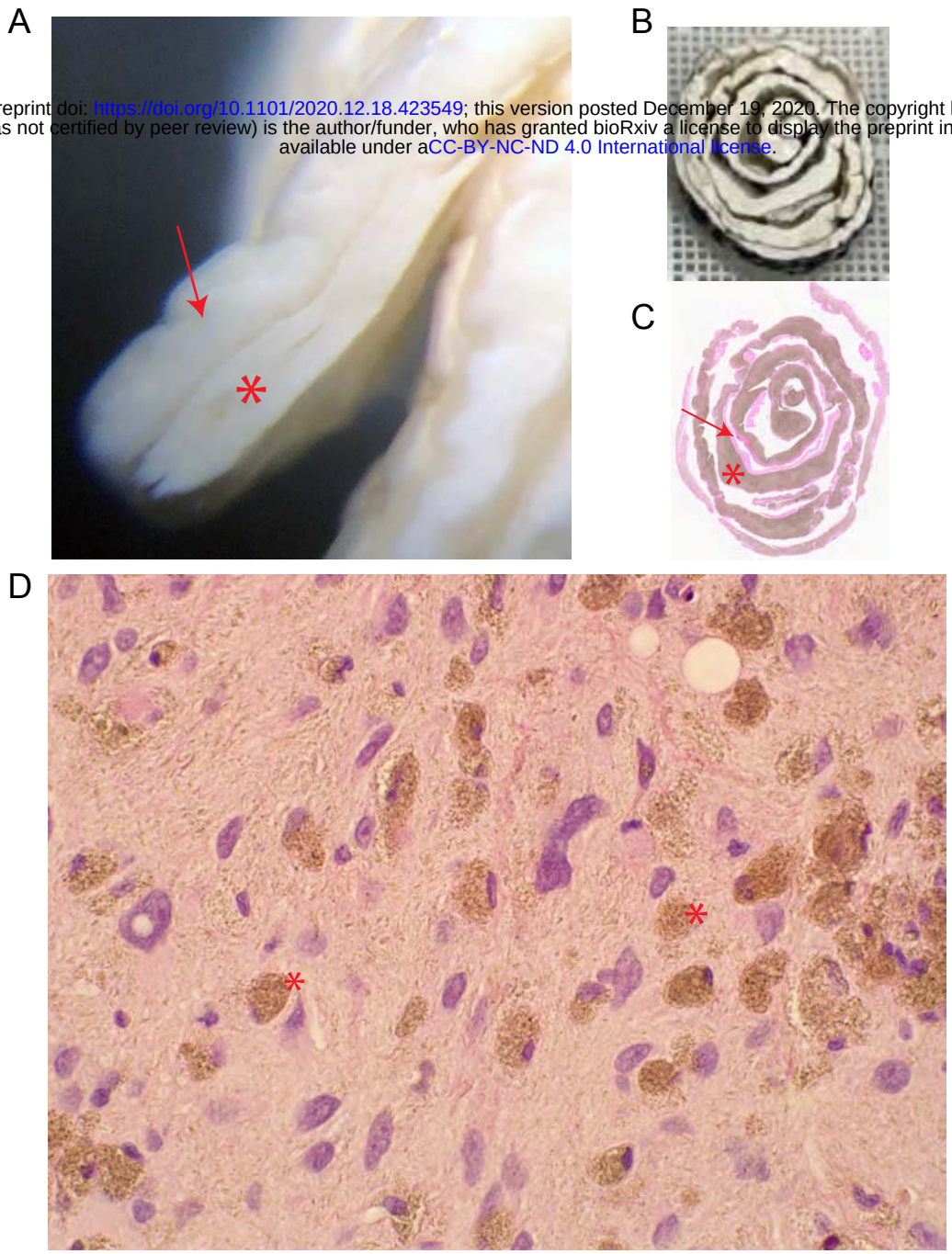

SupFig 3 Histopathology of skin tumors. (A) Thick layers of white tumor tissue (star) infiltrating white skin (arrow). (B) Skin biopsies organized and fixed in a paper roll for sectioning. (C) H&E staining of the skin sections. Arrow: skin; star: infiltrated tumor mass. (D) H&E staining of the skin sections showing normal skin cells and neoplastic cells (star). Neoplastic cells have eccentric and condensed nuclei.

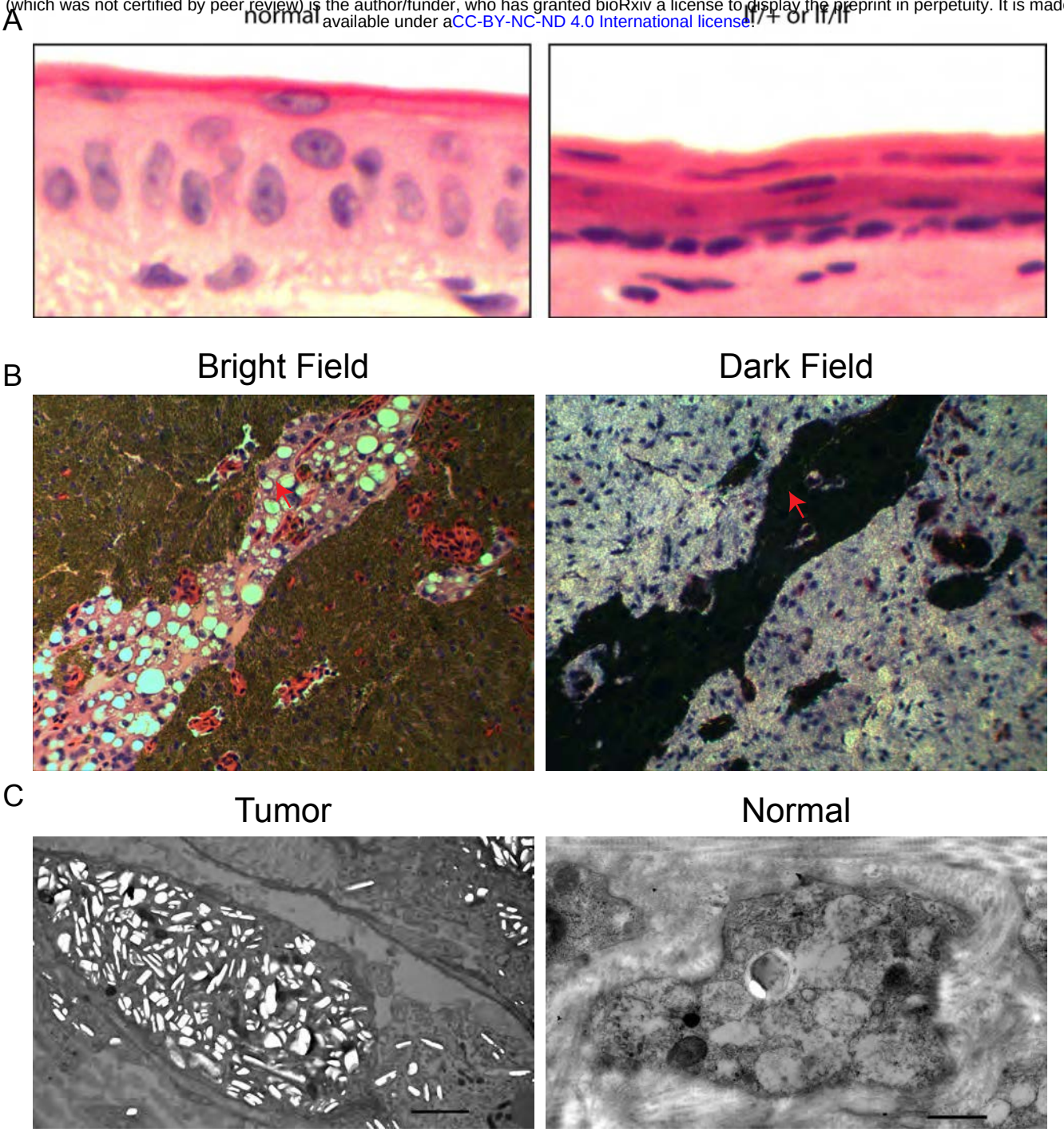

SupFig 4 Potential metastasis of iridophoroma. (A) In normal skin, cell nuclei are oval and perpendicular to the skin surface. In Lemon Frost skin, cell nuclei are flat, elongated and parallel to the skin, reminiscent of epithelial-to-mesenchymal transition. (B) ridophoroma in the liver, stained dark in H&E sections. In dark field imaging, iridophores are bright white. Such iridophores invade blood vessels in the tissue (red arrows). (C) n TEM imaging, white tumor skins in super LF are filled with abundant iridophores with excessive brightly reflective crystals (Tumor). In normal skin, iridophores are much fewer and have less crystals (Normal).

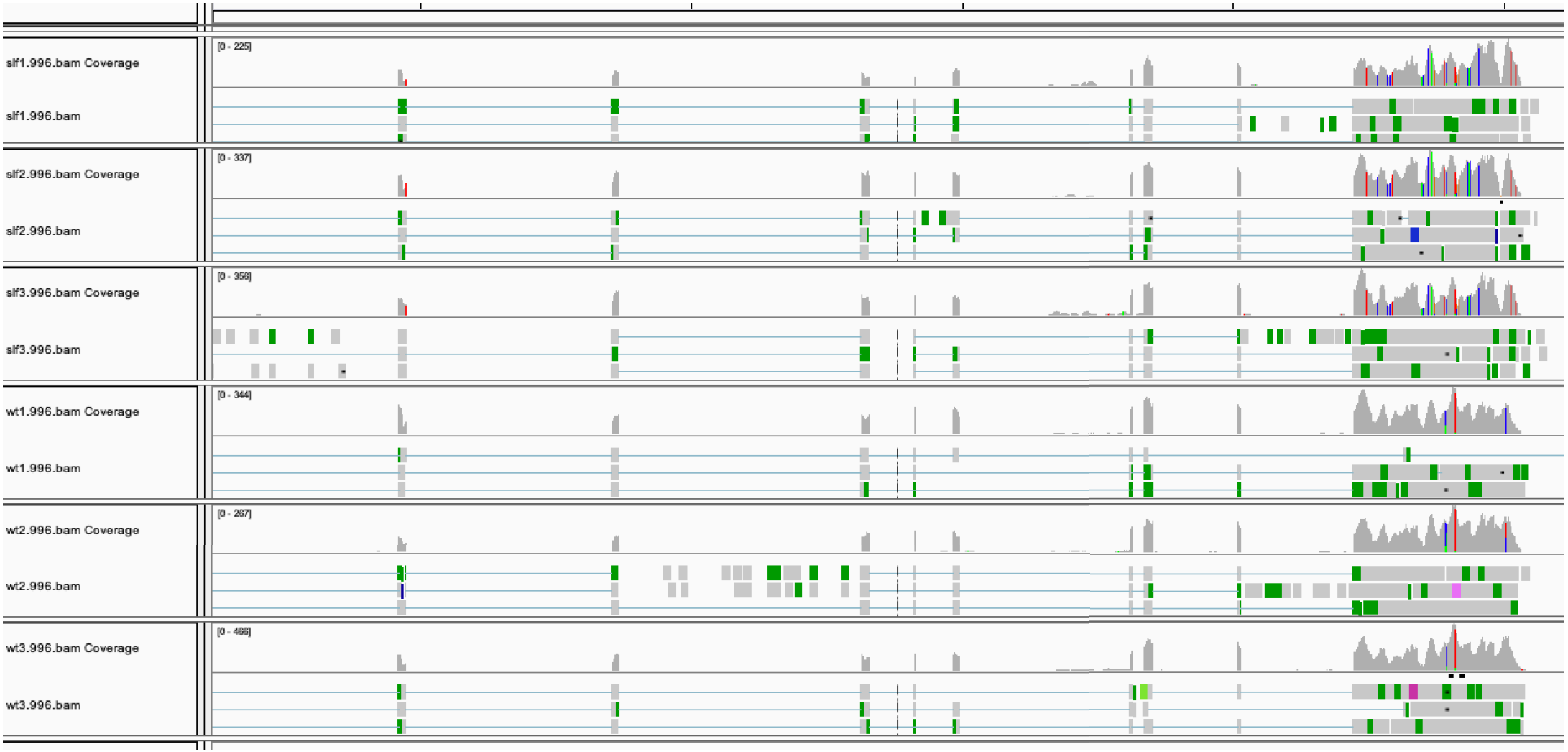

SupFig 5 SPINT1 expression in gecko skin. SPINT1 mRNA reads from transcriptome sequencing were aligned to the genome and visualized in IGV. Top 3 rows show samples from homozygous mutants. Bottom rows show samples from wild type geckos. Skin tissue adjacent to the tumors was used in the mutants. Peaks mark SPINT1 exons. The last exon on the right is transcribed together with the 3'UTR.